Journal of Thermal Analysis and Calorimetry
https://doi.org/10.1007/s10973-024-13501-0

Effect of CSH-PCE nanocomposites on early hydration of the ternary binder containing Portland cement, limestone, and calcined coal gangue

Ying Liu[1] · Qinghui Yang[1] · Yuantao Wang[1] · Shufeng Liu[1] · Yuanyuan Huang[1] · Delu Zou[1] · Xueyan Fan[1] · Haoran Zhai[1] · Yongling Ding[2]

Received: 4 April 2024 / Accepted: 9 July 2024

Abstract
In this work, the impact of lab synthetic addition agent, CSH-PCE nanocomposites (CPNs), on the early hydration property of the ternary binder containing Portland cement, limestone, and calcined coal gangue was investigated. CPNs were added in partial substitution of Portland cement by mass at 0%, 0.5%, 1.0%, 1.5%, 2.0%, 2.5% and 3.0%. X-ray diffraction (XRD), isothermal calorimetry, mercury intrusion porosimetry, and scanning electron microscopy were used to characterize the hydration and hydrates of the CPNs-modified pastes systematically. The workability and compressive strength of this ternary system was also studied. The obtained results indicated that the use of CPNs continuously improved the workability of the ternary mortar. The compressive strength of the ternary mortar increased with CPNs additions until the threshold limits of 3.0% and 2.5% before and after 12 h, under which the strength values were even higher than the reference OPC mortar at each age. Isothermal calorimetry results indicated that CPNs promoted cement hydration and produced more hydrates, which were also verified by the qualitative XRD analysis. This promotion effect leads to significant reduction in porosity as well as densification in microstructure within the ternary paste, ultimately resulting in enhanced early-age compressive strength. These findings provide valuable insights for designing lower carbon footprint ternary blends incorporating calcined coal gangue and limestone while maintaining comparable early-age compressive strength to traditional cement.

Keywords CSH · Nanocomposites · Calcined coal gangue · Hydration · Strength

Introduction

It is well known that during the cement production, a large volume of natural resources needs to be consumed and vast amounts of greenhouse gas is emitted as well during its manufacture. Extensive research indicates that the utilization of supplementary cementitious materials (SCMs) represents one of the most effective strategies for mitigating the environmental impacts associated with the cement industry, thereby facilitating the transition toward a resource-efficient and low-carbon economy [1, 2]. Furthermore, these materials greatly enhance the strength and durability of cement-based materials, contributing to their overall improvement [3, 4]. The Coal gangue (CG) is a kind of by-product generated from the process coal mining and washing, constituting approximately 10–20% of coal production [5]. Over the past decades, CG has been commonly disposed in landfills or as ponds, causing significant environmental issues. CG contains SiO_2, Al_2O_3, CaO and Fe_2O_3 as its main chemical components, making it a potential candidate for SCM [6]. Recent research indicates that unlike other SCMs used directly in cement-based materials, CG exhibits excellent pozzolanic activity after being calcined within an optimal temperature range [7]. The calcined CG, abbreviated as CCG, owns amorphous mineral, metakaolin (MK) [8].

At present, limestone calcined clay cement (LC^3) is popular studied. It is a type of low carbon cement consisting of 50% cement clinker, 5% gypsum, 15% limestone, and 30% calcined clay [9, 10]. Like calcined clay, CCG also contains

✉ Haoran Zhai
zijunzhang2023@163.com

[1] Shandong Hi-Speed Urban and Rural Development Group CO., LTD, 19F, Building 5, Zhongrun Century Wealth Center, No. 13873 Jingshi Road, Lixia District, Jinan 250014, People's Republic of China

[2] Shandong Jiaotong University, Jinan 250357, People's Republic of China

Published online: 03 September 2024

MK, therefore, the studies about the binders containing limestone, CCG and cement are increasing [11–13]. The utilization of 10–20% CCG alone leads to a slightly reduction in the compressive strength of cement mortar at both 7 and 28 d [11]. However, when the same amount of cement is replaced, the co-utilization of CCG and limestone enhances the strength of cement mortar at both 7 and 28 d [11, 12]. It should be noted that the compressive strength of cement mortar significantly decreases with the increasing content of CCG. The reactivity of CCG in the blended system is limited. However, when CCG is combined with limestone, the interaction between alumina phase and limestone leads to enhanced formation of carboaluminates and refinement of the pore structure in cement-based materials.

The incorporation CCG and limestone in a synergistic manner positively influences the strength development of cement, starting from 7 d. However, this ternary system exhibits relatively low early compressive strength. For instance, at 1 d, the compressive strength of cement paste mixed with 20% CCG and 10% limestone was reduced by 46.6% compared to the reference OPC [11]. Similar findings were also reported in the work of Li et al. [12], where using the same replacement level resulted in a reduction in compressive strength by 37.6% and 16.4% at 1 d and 3 d, respectively. CCG is a slow reacting materials at early curing time, the decrease in the cement content cannot be balanced by the CCG reactions. In addition, the participation of limestone in the reactions is also limited during this period. Therefore, it is imperative to address these detrimental effects since the strength and durability characteristics of concrete during early curing time are crucial in construction applications such as precast concrete.

It has been widely reported that many types of nano-materials are adopted to enhance the initial properties of cement-based materials, such as nano-SiO_2 [14, 15], nano-TiO_2 [16, 17], nano-$CaCO_3$ [18, 19], carbon nanotube/nanofiber [20–23], nano graphene [24, 25] and calcium silicate hydrate (CSH) seeds. Of the above nano-materials, CSH has recently become a research hotspot [26, 27]. CSH is one of the main hydrates from silicate minerals in Portland cement and it is also the primary phase contributing to the strength development of cement-based materials. When CSH seeding is applied, the early hydration of cement is greatly accelerated and compressive strength was also significantly enhanced [28, 29]. Several studies have reported that CSH seeding nanocomposites prepared by combining CSH and comb-like polymers, such as polycarboxylate superplasticizer (PCE), is more effective for enhancing cement hydration than pure CSH. This is because this type of nanocomposites are able to alleviate the agglomeration of CSH particles. Kanchanason et al. [30] investigated the influence of 2 mass% CSH-PCE nanocomposites on the compressive strength of cement blended with 35 mass% slag or calcined clay. It was found that this system exhibited a significant increase in strength, with an enhancement of approximately 240% at 16 h and a range of 25–95% from 1 to 28 d. Sun et al. [31] reported that the optimum addition of CSH-PCE nanocomposites in the blended cement with 20 mass% of metakaolin was 3 mass%, under which the compressive strength of this system was increased approximately 36%, 21% and 14% at 1, 3 and 7 d, respectively. The authors ascribed the increase in the strength to the enhancement of CSH-PCE nanocomposites on cement hydration and metakaolin reaction.

In this study, the effect of synthetic CSH-PCE nanocomposites (CPNs) on early hydration properties of the binders containing Portland cement, limestone, and calcined coal gangue are explored. The fluidity of fresh mortars was initially assessed, followed by compressive strength testing up to 7 d. Subsequently, the kinetics of hydration, phase assemblages, and microstructure were comprehensively analyzed using isothermal calorimetry, X-ray diffraction (XRD), scanning electron microscopy (SEM), and mercury intrusion porosimetry (MIP).

Materials and method

Material

A commercial CEM II-42.5 Portland cement (OPC) was produced from Fushun Cement Factory (Liaoning, China). Coal gangue was collected from Huainan Coal Mine (Anhui, China). Calcined coal gangue (CCG) was obtained by calcining coal gangue at 800 °C for 2 h. Limestone with a purity of 85% was sourced from Zaozhuang (Shandong, China). The chemical composition of these materials determined by X-ray fluorescence analysis is presented in Table 1. Their particle size distributions determined by laser particle size analyzer are depicted in Fig. 1. Additionally, dihydrate gypsum purchased from Taitan Chemical Reagent Co., Ltd

Table 1 Chemical composition of cement, limestone, and calcined coal gangue (mass%)

Oxides	Cement	Limestone	Calcined coal gangue
SiO_2	20.94	5.2	64.3
Al_2O_3	4.85	2.4	28.8
Fe_2O_3	3.44	1.3	3.1
CaO	64.02	55.6	0.5
MgO	1.70	2.7	0.5
SO_3	1.88	0.2	0.4
R_2O	0.50	0.63	1.5
f-CaO	0.50	–	–
L.O.I	1.88	31.6	–

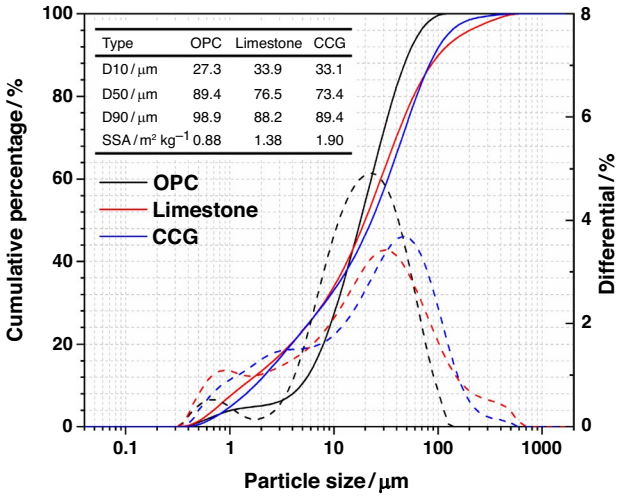

Fig. 1 Particle size distributions (PSD) of OPC, limestone, and CCG

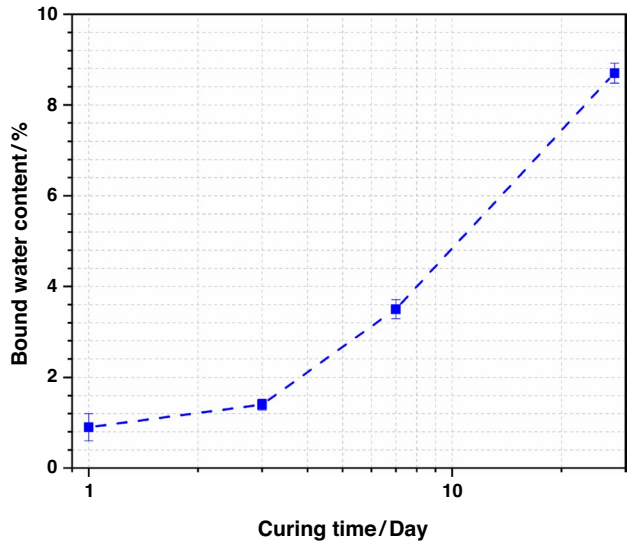

Fig. 2 Bound water content in the CCG-hydrated sample at different curing ages

(Shanghai, China) was utilized to adjust the sulfate content in the ternary binders containing CCG. In addition, R^3 test [32] was also adopted to evaluate the pozzolanic reactivity of CCG, which was expressed by the bound water content up to 7 d and the result is shown in Fig. 2. It can be seen that the bound water content increased obviously from 3 d, indicating the starting reaction of CCG with CH during this period, and this reaction was more intense with increasing the curing age.

The solid content of CPNs in the prepared solution is about 20% and the Ca/Si ratio in CPNs was 1.21. In addition, the Na content in CPNs could also be ignored since the excess Na has been filtered and washed away during the preparation process. The morphology of the sample was examined using transmission electron microscopy (TEM), as depicted in Fig. 3. As observed, CPNs particles with nanoscale was successfully prepared, and their average particles sizes were within 20 nm.

Mixtures design

The detailed proportions of the mortar mixtures are presented in Table 2. In this experiment, the reference ternary binder was obtained by mixing 69.6 mass% of cement, 20 mass% of calcined coal gangue, 10 mass% of limestone and 0.4 mass% of gypsum. The dosage of CPNs, a suspension with 20% solid content, was set from 0 to 3.0 mass% of binder (binder = cement + LC + CCG + gypsum) with a step of 0.5 mass%.

Preparation of paste and mortar samples

The paste samples were prepared as follows: Raw materials were weighed according to Table 2, followed by mixing at a low speed for 60 s and then at a high speed for 30 s using NJ-160B blender. The fresh mixtures were poured into plastic bottles with sizes of Φ 10 mm × 50 mm, then the pastes and bottles were manually vibrated for 10 s to compact the pastes. Finally, the bottles filled with pastes were tightly

Fig. 3 TEM images of CPNs

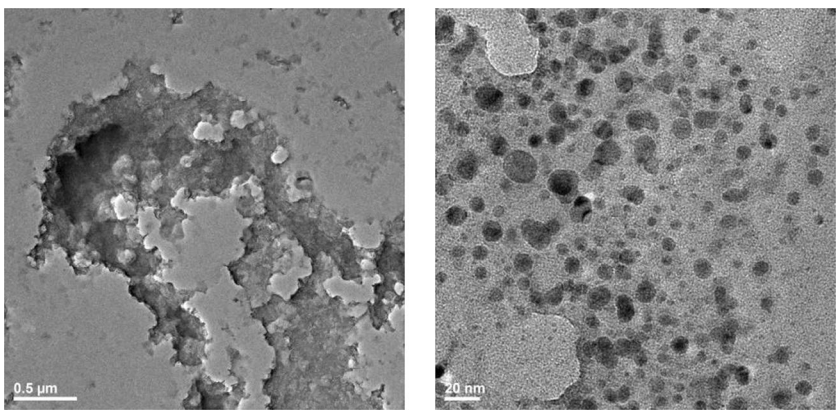

Table 2 Mixture proportions of studied systems (100 g basis)

Nomenclature	Cement	LS	CCG	CPNs	Gypsum	Theoretical water amount	Water introduced by CPNs	Additioal water
OPC	100	0	0	0	0	50	0	50
CCG20LS10	69.6	10	20	0	0.4	50	0	50
C0.5	69.1	10	20	0.5	0.4	50	2	48
C1.0	68.6	10	20	1.0	0.4	50	4	46
C1.5	68.1	10	20	1.5	0.4	50	6	44
C2.0	67.6	10	20	2.0	0.4	50	8	42
C2.5	67.1	10	20	2.5	0.4	50	10	40
C3.0	66.6	10	20	3.0	0.4	50	12	38

sealed with plastic cling film and placed in a standard curing room (20 °C, humidity above 95%). At the designated curing time, the pastes were carefully extracted from the bottles, fragmented into small pieces, and subsequently immersed in ethanol to stop hydration. Following a 7 d immersion period, a portion of these fragments was finely ground into powders passing through 75 μm sieve before being subjected to XRD analysis after drying for at least 48 h at 40 °C in a vacuum oven. The remaining fragments were directly dried under identical conditions for MIP and SEM analysis.

As for the mortar samples preparation, a fixed standard sand to binder ratio of 3 was used. All materials were weighed according to Table 2 followed by mixing at a low speed for 120 s and high speed for 40 s using JJ-5 blender. After conducting the fluidity measurement, the fresh mortars were carefully poured into steel molds measuring 40 mm × 40 mm × 160 mm and subsequently subjected to a controlled vibration of 60 cycles on the dedicated vibrating table. Subsequently, the mortar samples were put in the same curing environment as the paste samples until for the compressive strength test.

Methods

Fluidity measurement of mortar samples was conducted using the mini-slump flow testing conforming to the Chinese standard GB/T 8077-2012. The average of three tests was reported as the final fluidity.

The compressive strength of mortar samples was determined in accordance with the Chinese standard GB/T 8077-2012, following a standardized procedure. The average of six tests was reported as the final compressive strength.

The hydration heat evolution of paste samples was monitored using a TAM Air 8 isothermal calorimeter. The experiment was conducted at a constant temperature of 20 °C, and the data were recorded for up to 24 h.

A Rigaku SmartLab 3000A X-ray diffractometer with copper radiation ($\lambda = 0.154$ nm) was used to analyze the phase assemblages of samples with curing age. The instrument operated at an applied voltage of 45 kV and current of 15 mA, while data collection occurred from an angular range of 5° to 65° (2θ) with a scanning rate of 5°/min.

Pore structures analysis in the samples was performed using a PoreMaster GT60 mercury intrusion porosimeter, which enabled probing pore sizes ranging from 0.0035 to 400 μm.

Morphological observations on the samples were carried out using a Nova NanoSEM450 scanning electron microscope (SEM) equipped with a W tungsten filament operating at an accelerating voltage of 15 kV. Prior to testing, the samples were coated with a thin layer of gold for improved conductivity.

Results and discussion

Fluidity

Figure 4 shows fluidity of the different mortars. As shown in Fig. 4, the fluidity of CCG20LS10 mortar was 10.4% lower than that of the reference OPC mortar. The reason for this is that CCG and limestone possess smaller particle sizes (Fig. 3, with a larger specific surface area), necessitating a greater amount of water to fully cover the surface of these particles. For the same amount of water, less free water could be acted as the lubrication layer and the friction between these particles was increased, resulting in a decreased fluidity [33, 34].

It can be seen that adding CPNs efficiently increased the fluidity of CCG20LS10 mortar, especially at a higher amount of CPNs. For example, when the mixing amount of CPNs was 0.5%, 1.0%, 1.5%, 2.0%, 2.5% and 3.0%, the mortar fluidity increased approximately up to 161, 185, 266, 279, 289 and 293 mm, respectively, increased by 3.8%, 19.6%, 71.6%, 79.7%, 84.8% and 89.0% compared with CCG20LS10. This is associated with the superplasticizer introduced by CPNs that can reduce water demand while

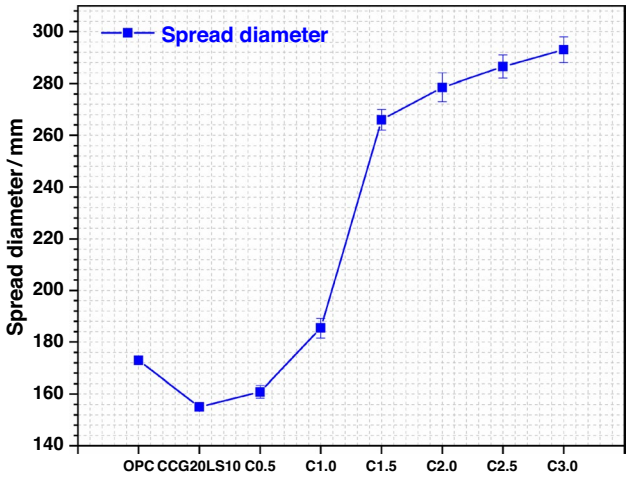

Fig. 4 The effect of CPNs on fluidity of the CCG20LS10 mortar

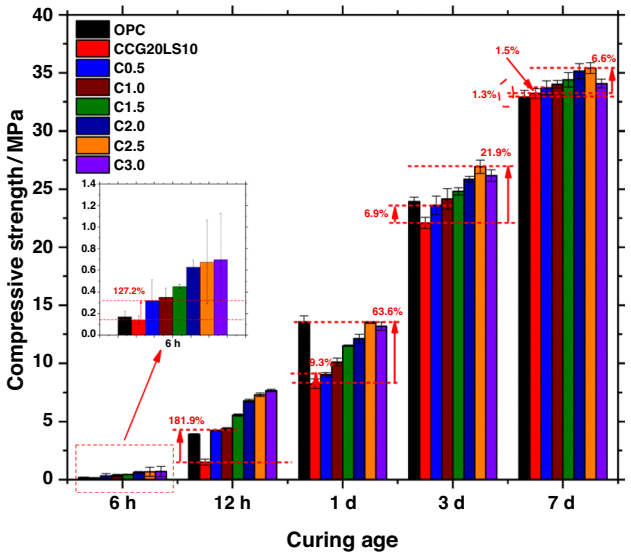

Fig. 5 Compressive strength of the specimens at different curing ages

maintaining adequate workability [35]. This observation is also completely different from other types of nano-particles, where higher amount of nano-particles resulted in much worse fluidity than the control mortars [24, 36].

Compressive strength

The compressive strength development for specimens at curing ages of 6 h, 12 h, 1 d, 3 d and 7 d is illustrated in Fig. 5. As displayed in Fig. 5, the specimen of CCG20LS10 experienced a much lower compressive strength than the reference OPC before 3 d. This is due to the much lower reactivity of CCG and limestone than that of cement at early ages, which resulted in precipitating less hydrates and thereby the slower progress in the compressive strength development. Such decrease in the compressive strength was less pronounced with increasing age. At the age of 7 d, the compressive strength of CCG20LS10 specimen was even about 1.3% higher than the reference OPC. Such a fast strength gain for CCG20LS10 specimen was associated with the starting reaction of CCG that produced more hydrates such as C–A–S–H and carboaluminates that greatly enhanced the corresponding compressive strength.

As expected, CPNs addition exhibited a directly positive effect on the compressive strength of CCG20LS10. The compressive strength of CCG20LS10 with CPNs was observed to increase as the content of CPNs increased before 12 h. The highest increase is observed in C3.0, where a significant enhancement in compressive strength is observed at 6 and 12 h, respectively, compared to CCG20LS10. The increase in the compressive strength due to the incorporation of CPNs can be attributed to their seeding effect, which greatly promotes cement hydration and facilitates the production of additional hydrates. In addition, CPNs particles possibly acted as fillers to fill the space in specimens, resulting in denser microstructures.

Similarly, compared with CCG20LS10, the increase in the compressive strength at 1, 3 and 7 d was observed to be 9.3–63.6%, 6.9–21.9% and 1.5–6.6% for the specimens with adding ranging from 0.5 to 3.0 mass%, respectively. It was observed from Fig. 4 that the maximum compressive strength of the specimen was obtained with CPNs at an amount of 2.5 mass% from 1 d onwards. The compressive strength, however, exhibited a decline upon further increase in the amount of CPNs up to 3.0 mass%, suggesting that an excessive presence of CPNs did not contribute favorably to the development of compressive strength in CCG20LS10.

Isothermal calorimetry

Figure 6 shows the isothermal calorimetry results of selected pastes up to 24 h. As shown in Fig. 6a, four hydration stages including initial reactions, induction period, acceleration period and deceleration period can be clearly seen in all pastes. Compared with CCG20LS10, the addition of CPNs shortened the induction period, which decreased continuously from around 2.9 to 1.8 h when CPNs additions increased from 0 to 3.0%. The acceleration period exhibits an exothermic peak, which is attributed to the hydration of Alite and the precipitation of CSH and calcium hydroxide (CH) [37]. It is visible that CPNs fastened the appearance of this peak and increased the corresponding peak intensity. For example, the hydration peak in the acceleration period occurred at around 13.2 h and its intensity was 0.0022 W g^{-1}. When 1%, 2% and 3% of CPNs was added, the occurrence of alite hydration peak shifted to approximately 5.4 h and the peak intensities increased up to 0.00265, 0.0034 and 0.00395

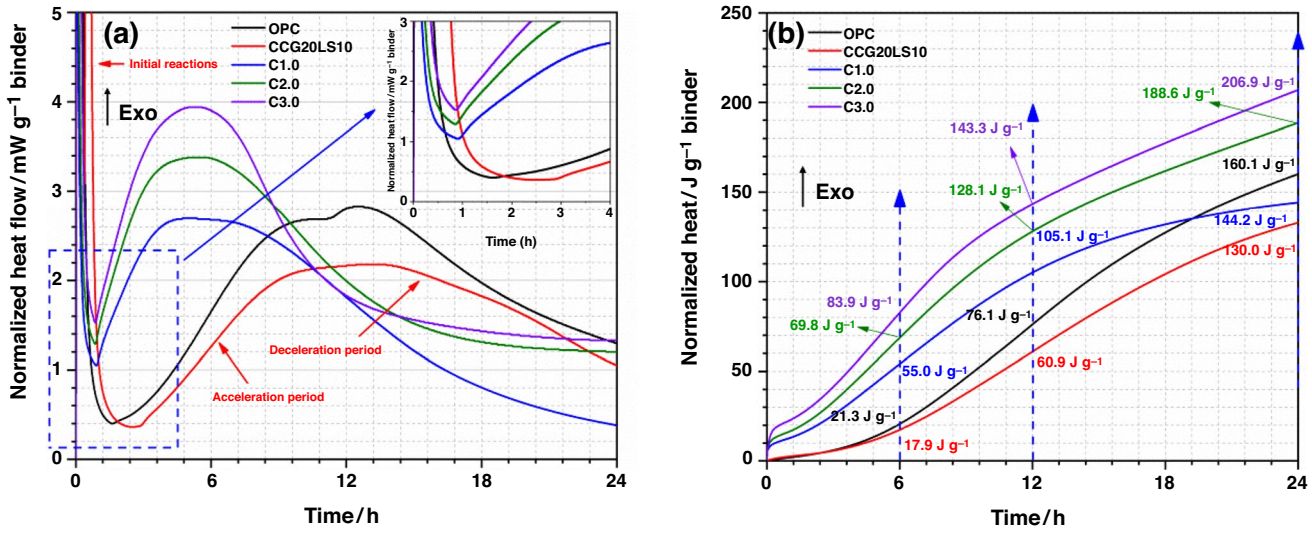

Fig. 6 Heat flow (**a**) and cumulative heat released (**b**) of the selected pastes normalized by the mass of selected pastes

W g^{-1}, respectively. This acceleration is associated with the nucleation sites effect of CPNs that enhances cement hydration, especially at higher CPNs additions.

Figure 6b shows the measured cumulative heat released of the pastes. The total hydration heat of CCG20LS10 at 6, 12, and 24 h exhibited a reduction of 16.0%, 20.0%, and 18.8% compared to the reference OPC. This is because CCG and limestone exhibit much lower reactivity at early ages than OPC, and the heat generated from the reactions relating to these two minerals are far from balancing the decreased hydration heat resulting from the decreased cement content. When CPNs was added, the total heat released of CCG20LS10 increased significantly. As shown in Fig. 6b, the total heat released of CCG20LS10 with 1%, 2% and 3% of CPNs increased by 207.3%, 289.9% and 368.7% at 6 h, 72.6%, 110.3% and 135.3% at 12 h, 9.4%, 45.1% and 59.2% at 24 h, respectively. It should be pointed out that CCG20LS10 with CPNs achieved even higher total hydration heat than that of the reference OPC (except C1.0 at 24 h). This observation was also well consistent with the compressive strength results.

X-ray diffraction analysis

Figure 7 displays the XRD patterns of CCG20LS10 samples with and without CPNs after different curing ages of hydration. In addition, XRD pattern of OPC is also given for better comparison. As displayed in Fig. 7, ettringite and CH respectively based on the peaks at 9.1° and 18.0° are the main crystalline hydrates of cement at all curing ages. In the samples of CCG20LS10 with or without CPNs, in addition to ettringite and CH, only the crystalline hydrate of hemicarboaluminate was formed (Fig. 7d–e).

It is well known that CH is precipitated from dicalcium silicate (C_2S) and tricalcium silicate (C_3S) hydration. In the ternary system with CCG and limestone, the pozzolanic reactivity of CCG and the synergistic effect between CCG and limestone would react with CH to precipitate C–A–S–H and carboaluminates (Hc in Fig. 5), respectively. Therefore, the CH, overlapped C_2S and C_3S, and Hc peaks respectively centered at 18.0°, 32.5° and 11.7° were selected for further comparison. The overlapped C_2S and C_3S peak intensity for the paste with CPNs was obviously lower than that of the CCG20LS10 paste, especially at higher CPNs addition, indicating that the addition of CPNs enhanced cement hydration. Meanwhile, compared with CCG20LS10, the intensity of CH peak in C1.0 at 6 and 12 h, C2.0 at 6 h was increased accordingly. However, in other cases, the intensity of this peak in CPNs-added pastes was decreased with increasing the amount of CPNs. This is possibly due to the enhanced reaction of CCG that consumed more CH. In addition, the Hc peak started to appear in CPNs-added CCG20LS10 sample from 3 d, indicating the addition of CPNs also enhanced the synergistic effect between CCG and limestone that precipitated more Hc. The qualitative XRD analysis revealed that the incorporation of CPNs not only enhanced cement hydration but also facilitated the reaction of CCG in CCG20LS10. More hydrates would produced in this process, which well supported the higher compressive strength development of the CPNs-added CCG20LS10 mortar.

Pore structure analysis

Figure 8 shows the porosity of OPC, CCG20LS10 samples with 0% and 2.5% of CPNs after different curing ages of

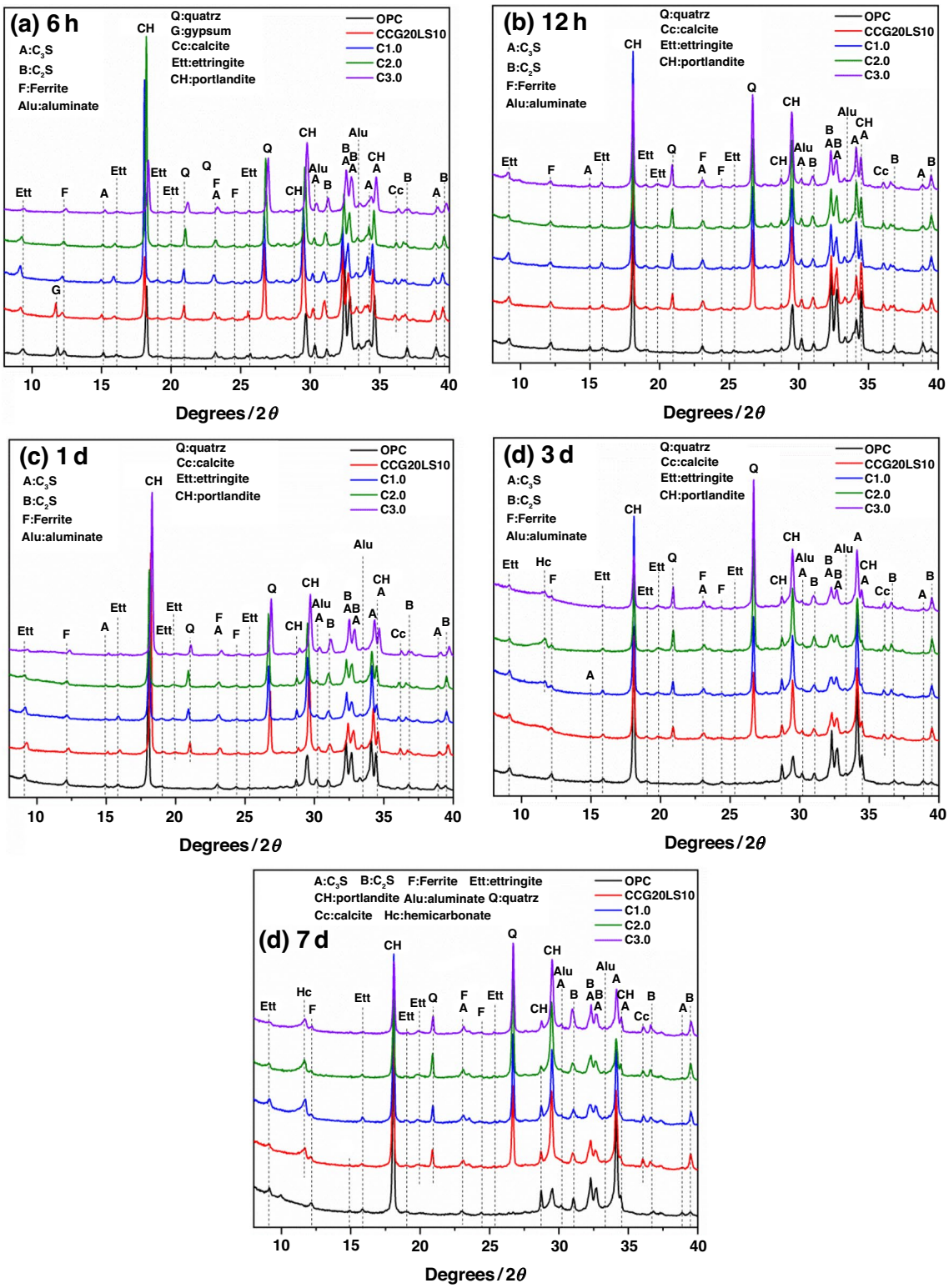

Fig. 7 XRD patterns of hydrated cement pastes at 6 h (**a**), 12 h (**b**), 1 d (**c**), 3 d (**d**) and 7 d (**e**)

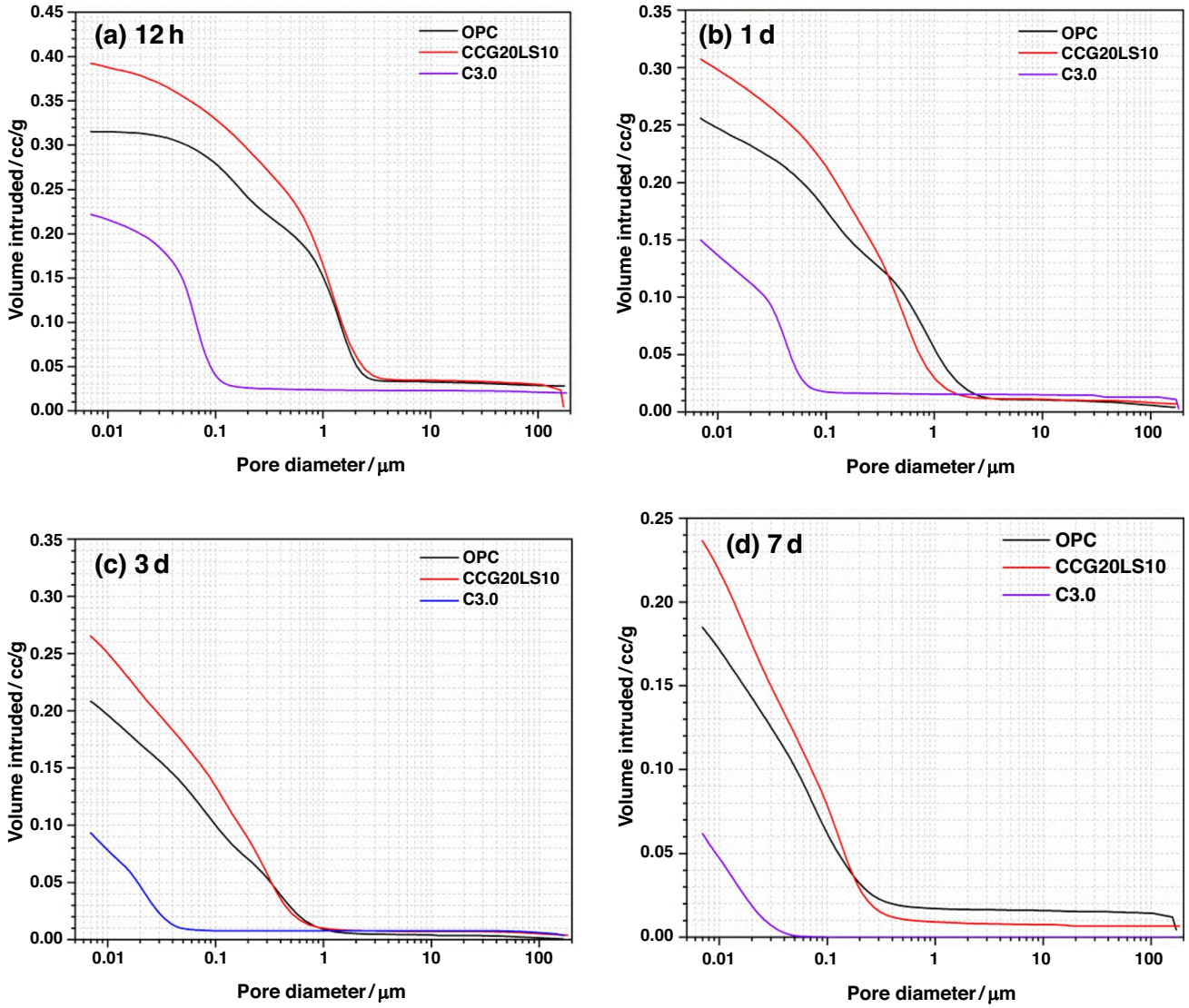

Fig. 8 Total porosity of selected systems at 12 h (**a**), 1 d (**b**), 3 d (**c**) and 7 d (**d**)

hydration. As the curing age increased, the porosity of each system decreased due to the continuous reactions, including cement hydration and the reaction of CCG.

The replacement of cement by CCG and limestone led to an increased porosity at all curing ages, as depicted in Fig. 8. For instance, compared to the reference OPC, the system of CCG20LS10 exhibited approximately 24.4%, 20.1%, 27.4%, and 27.9% increases in porosity at 12 h, 1 d, 3 d, and 7 d, respectively. This can be attributed to a higher water-to-cement ratio and lower gel-to-space ratio when cement was partially substituted with CCG and limestone, which is analogous to the scenario where fly ash was incorporated for partial cement replacement.

The addition of CPNs greatly improved the pore structure reflected by the significant decrease in the porosity at each curing age. This is likely associated with the seeding effect of CPNs that accelerated cement hydration, which produced more hydrates and efficiently decreased the porosity of CCG20LS10. In addition, the particle sizes of CPNs is much finer than that of cement, CCG and limestone particles, which can fill the pores and helped to decrease the porosity. It should be pointed out that as for the CPNs added system, it also exhibited about 29.6%, 41.4%, 55.2% and 57.1% decrease of porosity than the reference OPC at 12 h, 1 d, 3 d and 7 d, respectively. This observation also well explains the compressive strength results, where the mortar with adding 2.5% CPNs yielded significant higher compressive strength than both mortars of CCG20LS10 and OPC at each curing age.

Morphology observation

Morphology observation was performed on the samples of OPC, CCG20LS10 and C3.0 at 1 (Fig. 9) and 7 d (Fig. 10). It can be clearly seen that the typical hydrates such as CSH gel, AFt and CH were precipitated in hydrated OPC at 1 d (Fig. 9a), which is well consistent with the XRD observations (Fig. 7). In addition, many pores left by the free water were also observed. As for the CCG20LS10 paste, hydrates were easier to be observed (Fig. 9b), being associated with the filler effect of CCG and limestone that promoted cement hydration. However, its microstructure was less denser compared with OPC, which was reflected by more pores and disconnection of hydrates (Fig. 9e). This is

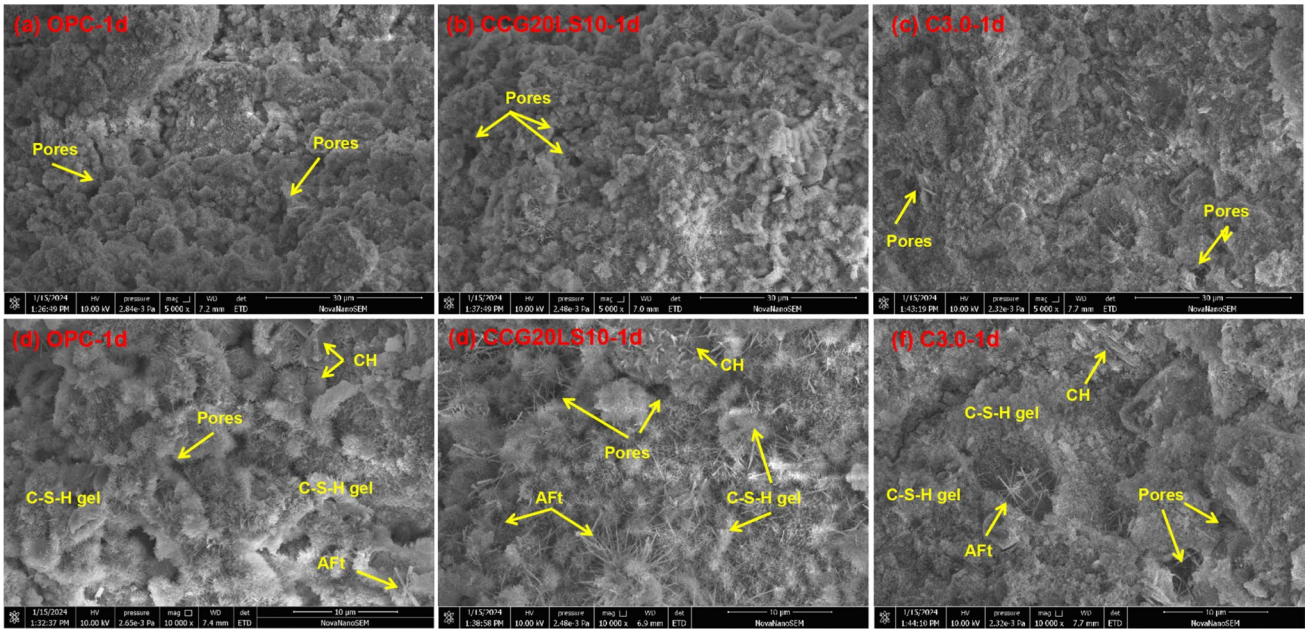

Fig. 9 SEM images of the selected samples at 1 d

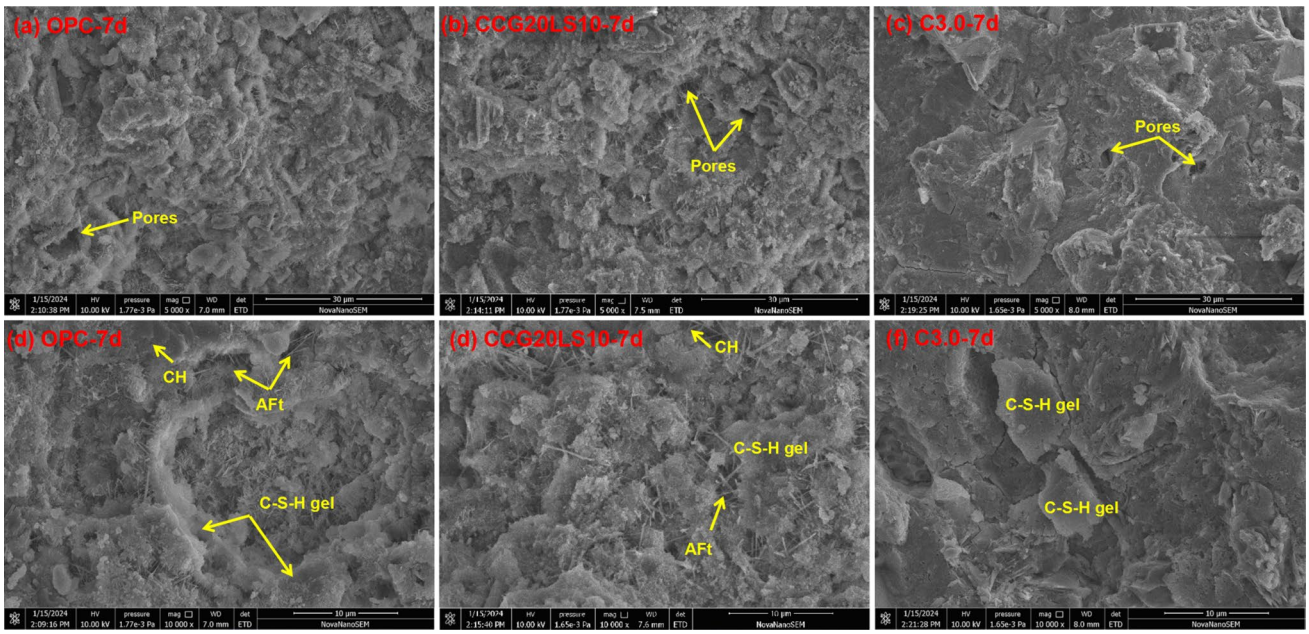

Fig. 10 SEM images of the selected samples at 7 d

due to the much lower reactivity of CCG and limestone than that of cement at early stage. On the contrary, the microstructure of C3.0 was dense and contained a few pores and fine hydrates, mainly due to the seeding effect of CPNs that has great contribution of early-age cement hydration. Understandably, C3.0 displays comparable strength to OPC but much higher than CCG20LS10 (Fig. 5).

After 7 d of hydration (Fig. 10), the microstructure of each system became denser due to the continuous reactions with forming more hydrates. The pozzolanic reaction of CCG and the synergistic interaction between CCG and limestone were found to be highly significant during this period, thereby facilitating the microstructural development of CCG20LS10 paste. This well explains the similar microstructure between OPC and CCG20LS10. From Fig. 10f, the hydrates in C3.0 were tightly connected with few pores, contributing to a much denser microstructure in comparison with OPC and CCG20LS10, evidenced by the MIP results in Fig. 8. This is associated with the acceleration effect of CPNs on the reactions in the sample of CCG20LS10 that produced more hydrates and compacted the microstructure, which well explains the highest compressive of C3.0 achieved at 7 d (Fig. 5).

Conclusions

The present study investigates the impact of synthetic CSH-PCE nanocomposites on the early hydration process of ternary binders comprising Portland cement, limestone, and calcined coal gangue. The fluidity, compressive strength, hydration heat, phase assemblages, and microstructure changes of the blends containing CSH-PCE nanocomposites were evaluated. Based on the aforementioned experimental findings, the following conclusions can be drawn:

1. The workability of the ternary mortar continuously increased with increasing the CPNs content up to 3.0%, which is due to the superplasticizer introduced by CPNs that can reduce water demand while maintaining adequate workability.
2. The incorporation of CPNs significantly enhanced the compressive strength of the ternary mortar at all curing ages. The highest compressive strength of the ternary mortar was achieved with a 3.0% dosage of CPNs at 6 and 12 h, and with a 2.5% dosage at 1, 3, and 7 d. Remarkably, even compared to the reference OPC mortar, the compressive strength of the ternary mortar surpassed it from as early as 6 h up to 7 d.
3. Isothermal calorimetry and qualitative XRD analysis revealed that the addition of CPNs not only enhanced cement hydration, but also facilitated the reaction of CCG. resulting in increased formation of hydrates in the ternary paste. These hydrates contributed to a significant reduction of porosity and densification of microstructure (evidenced by MIP and SEM observations), well supporting the compressive strength development.

Author contributions Haoran Zhai: Conceptualization; Ying Liu, Qinghui Yang, Yuantao Wang, Shufeng Liu, Yuanyuan Huang, Delu Zou, Xueyan Fan: Investigation; Yongling Ding: Writing.

Declarations

Conflict of interest The authors declare that they have no known competing financial interests or personal relationships that could have appeared to influence the work reported in this paper.

References

1. Snellings R, Suraneni P, Skibsted J. Future and emerging supplementary cementitious materials. Cem Conc Res. 2023. https://doi.org/10.1016/j.cemconres.2023.107199.
2. Pacewska B, Wilińska I. Usage of supplementary cementitious materials: advantages and limitations. J Therm Anal Calorim. 2020. https://doi.org/10.1007/s10973-020-09907-1.
3. Navarrete I, Valdes J, Lopez M, Vargas F. Replacement of pozzolanic blended cement by supplementary cementitious materials: mechanical and environmental approach. Constr Build Mater. 2023. https://doi.org/10.1016/j.conbuildmat.2023.132263.
4. Juenger MCG, Snellings R, Bernal SA. Supplementary cementitious materials: new sources, characterization, and performance insights. Cem Conc Res. 2019. https://doi.org/10.1016/j.cemconres.2019.05.008.
5. Liu X. Low-carbon utilization of coal gangue under the carbon neutralization strategy: a short review. J Mater Cycles Waste. 2023. https://doi.org/10.1007/s10163-023-01712-w.
6. Li J, Wang J. Comprehensive utilization and environmental risks of coal gangue: a review. J Clean Prod. 2019. https://doi.org/10.1016/j.jclepro.2019.117946.
7. Zhang Y, Ling T. Reactivity activation of waste coal gangue and its impact on the properties of cement-based materials: a review. Constr Build Mater. 2020. https://doi.org/10.1016/j.conbuildmat.2019.117424.
8. Xu B, Liu Q, Ai B, Ding S, Frost RL. Thermal decomposition of selected coal gangue. J Therm Anal Calorim. 2018. https://doi.org/10.1007/s10973-017-6687-4.
9. Zunino F, Martirena F, Scrivener K. Limestone calcined clay cements (LC^3). Aci Mater J. 2021. https://doi.org/10.14359/51730422.
10. Scrivener K, Avet F, Maraghechi H, Zunino F, Ston J, Hanpongpun W, Favier A. Impacting factors and properties of limestone calcined clay cements (LC^3). Green Mater. 2019. https://doi.org/10.1680/jgrma.18.00029.
11. Liu Y, Ling TC, Wang M, Wu YY. Synergic performance of low-kaolinite calcined coal gangue blended with limestone in cement mortars. Constr Build Mater. 2021. https://doi.org/10.1016/j.conbuildmat.2021.124012.
12. Li L, Zhang Y, Liu Y, Ling TC. Upcycling coal- and soft-series metakaolin in blended cement with limestone. Constr Build Mater. 2022. https://doi.org/10.1016/j.conbuildmat.2022.126965.

13. Jiu S, Wang M, Chen Y, Chen Y, Gao Q. Synthesis and characterization of low-carbon cementitious materials from suspended calcined coal gangue. Front Mater. 2022. https://doi.org/10.3389/fmats.2022.982861.
14. Zhuang C, Chen Y. The effect of nano-SiO_2 on concrete properties: a review. Nanotechnol Rev. 2019. https://doi.org/10.1515/ntrev-2019-0050.
15. Balapour M, Joshaghani A, Althoey F. Nano-SiO_2 contribution to mechanical, durability, fresh and microstructural characteristics of concrete: a review. Constr Build Mater. 2018. https://doi.org/10.1016/j.conbuildmat.2018.05.266.
16. Yang F, Xie J, Wang W, Wang W, Wang Z. The role of nano-TiO_2 on the mechanical properties and hydration behavior of C_2S, C_3S and $C_4A_3S^{-}$. Constr Build Mater. 2023. https://doi.org/10.1016/j.conbuildmat.2023.131558.
17. Sun J, Tian L, Yu Z, Zhang Y, Li C, Hou G, Shen X. Studies on the size effects of nano-TiO_2 on Portland cement hydration with different water to solid ratios. Constr Build Mater. 2020. https://doi.org/10.1016/j.conbuildmat.2020.120390.
18. Cui K, Lau D, Zhang Y, Chang J. Mechanical properties and mechanism of nano-$CaCO_3$ enhanced sulphoaluminate cement-based reactive powder concrete. Constr Build Mater. 2021. https://doi.org/10.1016/j.conbuildmat.2021.125099.
19. Sharma H, Ashish DK. Nano $CaCO_3$ for enhancing properties of cement-based materials: a comprehensive review. J Sustainable Cem-Based Mater. 2023. https://doi.org/10.1080/21650373.2023.2233512.
20. MacLeod AJN, Collins FG, Duan W. Effects of carbon nanotubes on the early-age hydration kinetics of Portland cement using isothermal calorimetry. Cem Conc Compos. 2021. https://doi.org/10.1016/j.cemconcomp.2021.103994.
21. Song C, Hong G, Choi S. Effect of dispersibility of carbon nanotubes by silica fume on material properties of cement mortars: Hydration, pore structure, mechanical properties, self-desiccation, and autogenous shrinkage. Constr Build Mater. 2020. https://doi.org/10.1016/j.conbuildmat.2020.120318.
22. Öksüzer N, Anil Ö, Aldemir A, Şahmaran M. Investigation of mechanical properties of high-performance hybrid fiber concretes adding nanomaterials using with coarse aggregate. Structures. 2021. https://doi.org/10.1016/j.istruc.2021.06.044.
23. Parveen S, Rana S, Fangueiro R. A review on nanomaterial dispersion, microstructure, and mechanical properties of carbon nanotube and nanofiber reinforced cementitious composites. J Nanomater. 2013. https://doi.org/10.1155/2013/710175.
24. Mowlaei R, Lin J, Basquiroto de Souza F, Fouladi A, Korayem AH, Shamsaei E, Duan W. The effects of graphene oxide-silica nanohybrids on the workability, hydration, and mechanical properties of Portland cement paste. Constr Build Mater. 2021. https://doi.org/10.1016/j.conbuildmat.2020.121016.
25. Mokhtar MM, Abo-El-Enein SA, Hassaan MY, Morsy MS, Khalil MH. Mechanical performance, pore structure and micro-structural characteristics of graphene oxide nano platelets reinforced cement. Constr Build Mater. 2017. https://doi.org/10.1016/j.conbuildmat.2017.02.021.
26. John E, Matschei T, Stephan D. Nucleation seeding with calcium silicate hydrate: a review. Cem Conc Res. 2018. https://doi.org/10.1016/j.cemconres.2018.07.003.
27. Cuesta A, Morales-Cantero A, De la Torre AG, Aranda MAG. Recent advances in C–S–H nucleation seeding for improving cement performances. Materials. 2023. https://doi.org/10.3390/ma16041462.
28. Morales-Cantero A, Cuesta A, De la Torre AG, Santacruz I, Mazanec O, Borralleras P, Weldert KS, Gastaldi D, Canonico F, Aranda MAG. C–S–H seeding activation of Portland and Belite cements: an enlightening in situ synchrotron powder diffraction study. Cem Conc Res. 2022. https://doi.org/10.1016/j.cemconres.2022.106946.
29. Li X, Bizzozero J, Hesse C. Impact of C-S-H seeding on hydration and strength of slag blended cement. Cem Conc Res. 2022. https://doi.org/10.1016/j.cemconres.2022.106935.
30. Kanchanason V, Plank J. Effect of calcium silicate hydrate-polycarboxylate ether (C-S-H–PCE) nanocomposite as accelerating admixture on early strength enhancement of slag and calcined clay blended cements. Cem Conc Res. 2019. https://doi.org/10.1016/j.cemconres.2019.01.007.
31. Sun J, Dong H, Wu J, Jiang J, Li W, Shen X, Hou G. Properties evolution of cement-metakaolin system with C-S-H/PCE nanocomposites. Constr Build Mater. 2021. https://doi.org/10.1016/j.conbuildmat.2021.122707.
32. Avet F, Snellings R, Alujas Diaz A, Ben Haha M, Scrivener K. Development of a new rapid, relevant and reliable (R3) test method to evaluate the pozzolanic reactivity of calcined kaolinitic clays. Cem Concr Res. 2016. https://doi.org/10.1016/j.cemconres.2016.02.015.
33. Burroughs JF, Weiss J, Haddock JE. Influence of high volumes of silica fume on the rheological behavior of oil well cement pastes. Constr Build Mater. 2019. https://doi.org/10.1016/j.conbuildmat.2019.01.027.
34. Jing W, Wu F, Yang J, Yin J, Ji W. Effects of silica fume and TiO_2 on properties of MKPC based fire retardant coatings for steel structure. Bulletin of the Chinese Ceramic Society. 2020. In Chinese.
35. Saeed NM, Omer B, Jamal AS, Dheyaaldin MH. Performance of cement mortar modified with GGBFS at elevated temperatures with various w/b ratios and superplasticizer dosages. Constr Build Mater. 2023. https://doi.org/10.1016/j.conbuildmat.2023.130493.
36. Collins F, Lambert J, Duan WH. The influences of admixtures on the dispersion, workability, and strength of carbon nanotube-OPC paste mixtures. Cem Conc Compos. 2012. https://doi.org/10.1016/j.cemconcomp.2011.09.013.
37. Zunino F, Scrivener K. The influence of the filler effect on the sulfate requirement of blended cements. Cem Conc Res. 2019. https://doi.org/10.1016/j.cemconres.2019.105918.